Electronic Supplementary Material (ESI) for New Journal of Chemistry.
This journal is © The Royal Society of Chemistry and the Centre National de la Recherche Scientifique 2021.

Supporting Information

Nanospheres from coordination polymers of Ag^+ with a highly hydrophilic thiol ligand *in situ* formed from dynamic covalent binding and a hydrophobic thiol

Yan Xu,[a] Xiao-Sheng Yan,[a] Si-Bo Zhang,[b] Shao-Wei Li,[b] Ning-Shao Xia,[b] Tao Jiang,[a] Zhao Li[a] and Yun-Bao Jiang*,[a]

[a] Department of Chemistry, College of Chemistry and Chemical Engineering, the MOE Key Laboratory of Spectrochemical Analysis and Instrumentation, and *i*ChEM, Xiamen University, Xiamen 361005, China.

[b] State Key Laboratory of Molecular Vaccinology and Molecular Diagnostics, School of Life Sciences, School of Public Health, Xiamen University, Xiamen 361102, China; National Institute of Diagnostics and Vaccine Development in Infectious Disease, Xiamen University, Xiamen 361102, China

E-mail: ybjiang@xmu.edu.cn

Table of Contents

1. Supplementary Spectral Data

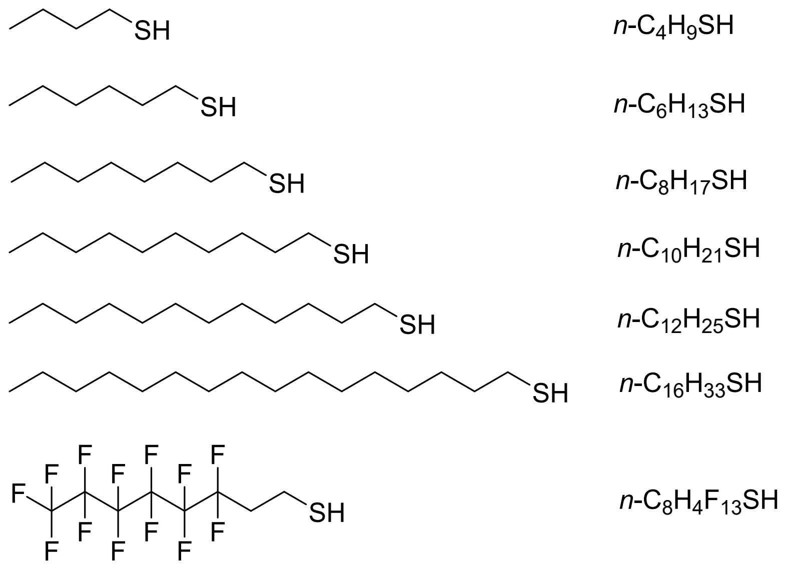

Scheme S1 Chemical structures of n-$C_nH_{2n+1}SH$ and their fluorinated derivative n-$C_8H_4F_{13}SH$.

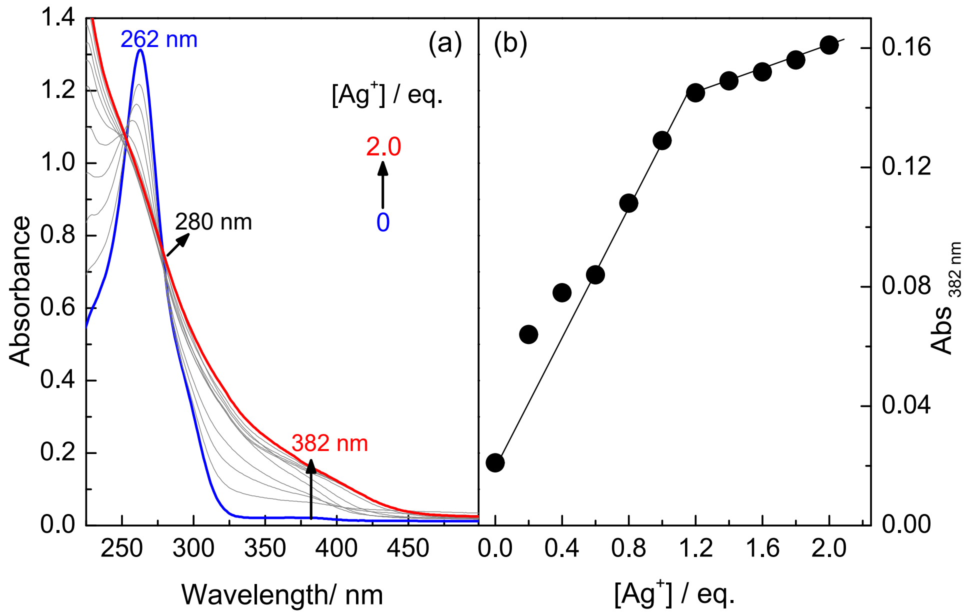

Fig. S1 (a) Absorption spectra of (4-MPBA+D-glucose) in the presence of Ag^+ of increasing concentration in 100 mM Na_2CO_3-$NaHCO_3$ buffer solution of pH 10.5 and (b) absorbance at 382 nm versus equivalent of Ag^+. [4-MPBA] = 100 μM, [D-glucose] = 3 mM, [Ag^+] = 0 - 2.0 eq.

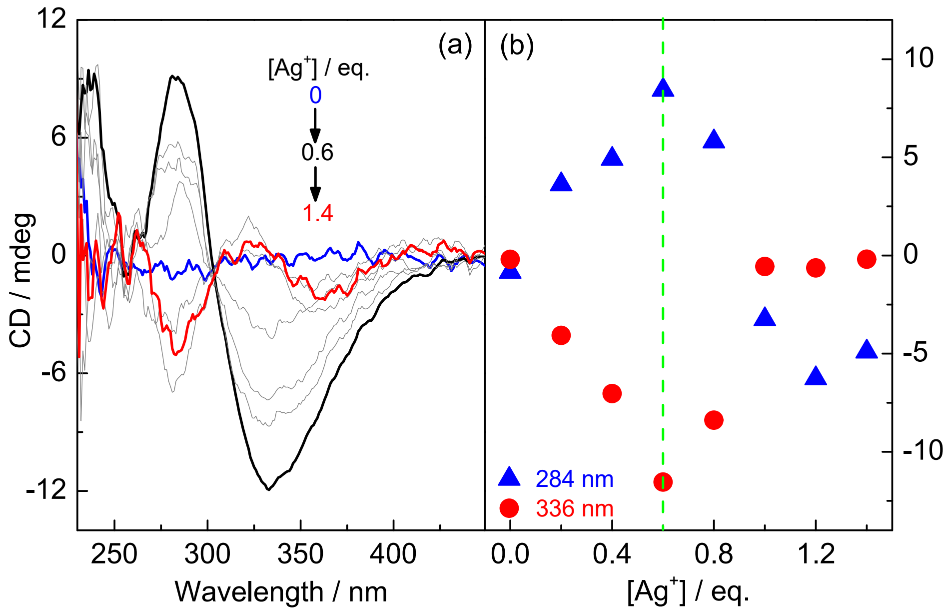

Fig. S2 (a) CD spectra (4-MPBA+D-glucose) in the presence of Ag^+ of increasing concentration in 100 mM Na_2CO_3-$NaHCO_3$ buffer solution of pH 10.5 and (b) plots of CD signals at 284 nm and 336 nm versus equivalent of Ag^+. [4-MPBA] = 100 μM, [D-glucose] = 3 mM, [Ag^+] = 0 - 1.4 eq. Note that in the absence of D-glucose the coordination polymers of Ag^+ with 4-MPBA are CD silent because there is no chiral element, despite their formation is suggested by variations in the absorption (Fig. S3).

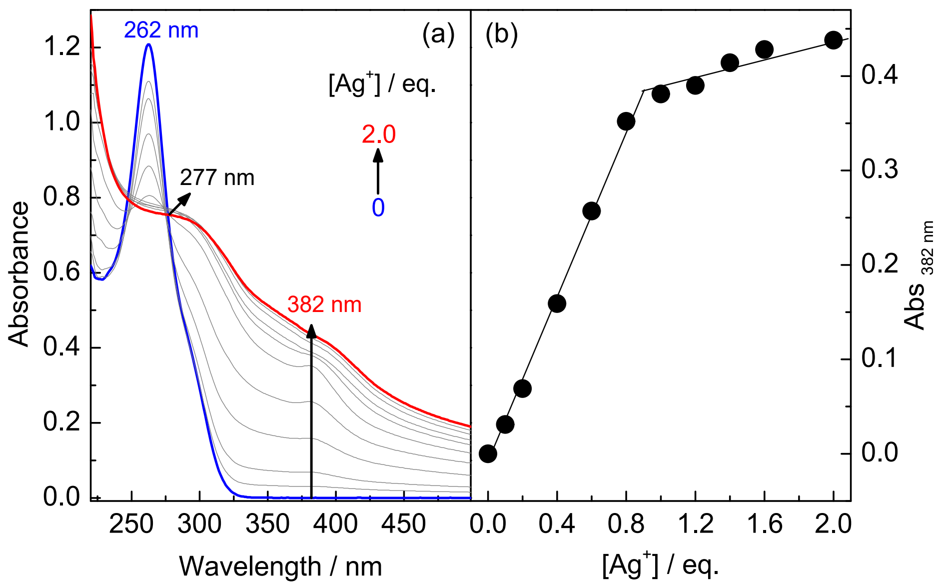

Fig. S3 (a) Absorption spectra of 4-MPBA in the presence of Ag^+ of increasing concentration in 100 mM Na_2CO_3-$NaHCO_3$ buffer of pH 10.5 and (b) plots of absorbance at 382 nm versus equivalent of Ag^+. [4-MPBA] = 100 μM, [Ag^+] = 0 - 2.0 eq.

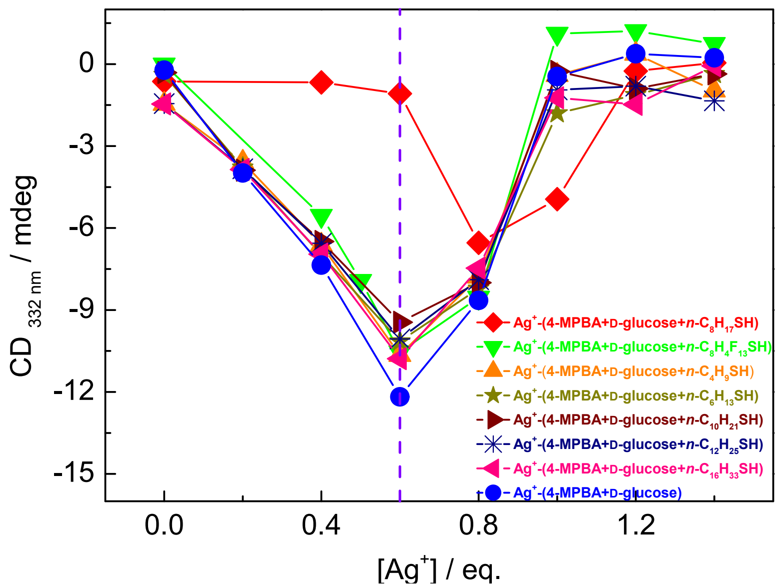

Fig. S4 Plots versus Ag^+ concentration of CD signal at 332 nm of Ag^+-(4-MPBA+D-glucose+*n*-$C_nH_{2n+1}SH$), Ag^+-(4-MPBA+D-glucose+*n*-$C_8H_4F_{13}SH$) and Ag^+-(4-MPBA+D-glucose) in 100 mM Na_2CO_3-$NaHCO_3$ buffer of pH 10.5. [4-MPBA] = 100 μM, [*n*-$C_nH_{2n+1}SH$] = 100 μM, [*n*-$C_8H_4F_{13}SH$] = 100 μM, [D-glucose] = 3 mM, [Ag^+] = 0 - 1.4 eq.

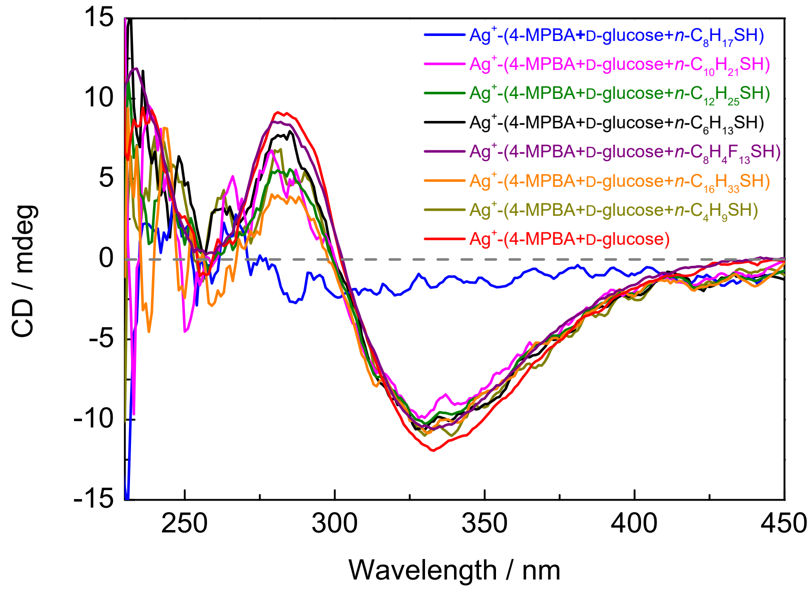

Fig. S5 CD spectra of Ag^+-(4-MPBA+D-glucose+*n*-$C_nH_{2n+1}SH$), Ag^+-(4-MPBA+D-glucose+*n*-$C_8H_4F_{13}SH$) and Ag^+-(4-MPBA+D-glucose) in 100 mM Na_2CO_3-$NaHCO_3$ buffer of pH 10.5. [4-MPBA] = 100 μM, [*n*-$C_nH_{2n+1}SH$] = 100 μM, [*n*-$C_8H_4F_{13}SH$] = 100 μM, [D-glucose] = 3 mM; [Ag^+] = 60 μM (red line), 120 μM (other lines).

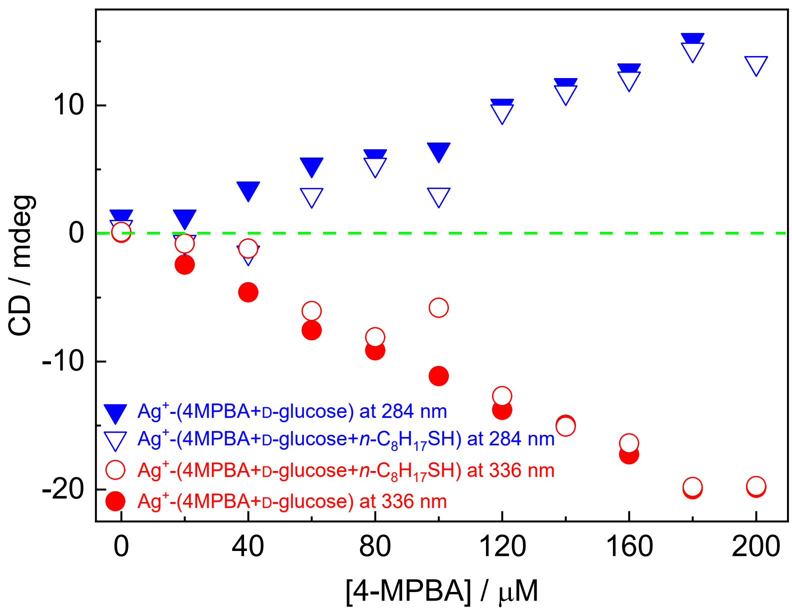

Fig. S6 Plots of CD signals of Ag^+-(4-MPBA+D-glucose) and Ag^+-(4-MPBA+D-glucose+n-$C_8H_{17}SH$) of varying concentration of 4-MPBA. [4-MPBA] = 0 - 200 μM (solid), [4-MPBA] + [n-$C_8H_{17}SH$] = 200 μM (hollow), [D-glucose] = 3 mM.

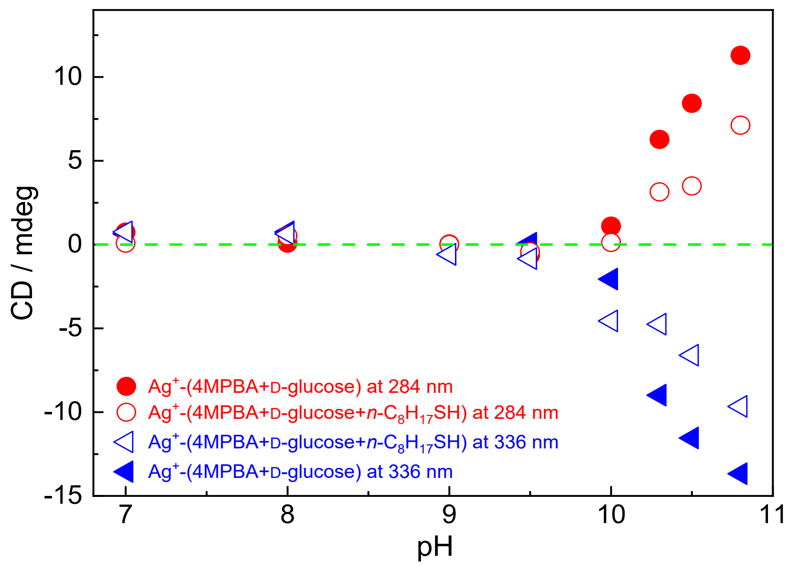

Fig. S7 Plots of CD signals of Ag^+-(4-MPBA+D-glucose) and Ag^+-(4-MPBA+D-glucose+n-$C_8H_{17}SH$) in solutions of varying the pH. [4-MPBA] = 100 μM, [n-$C_8H_{17}SH$] = 100 μM, [D-glucose] = 3 mM; [Ag^+] = 60 μM (solid), 160 μM (hollow). pH = 7, 8, 9, 9.5, 10, 10.3, 10.5, or 10.8.

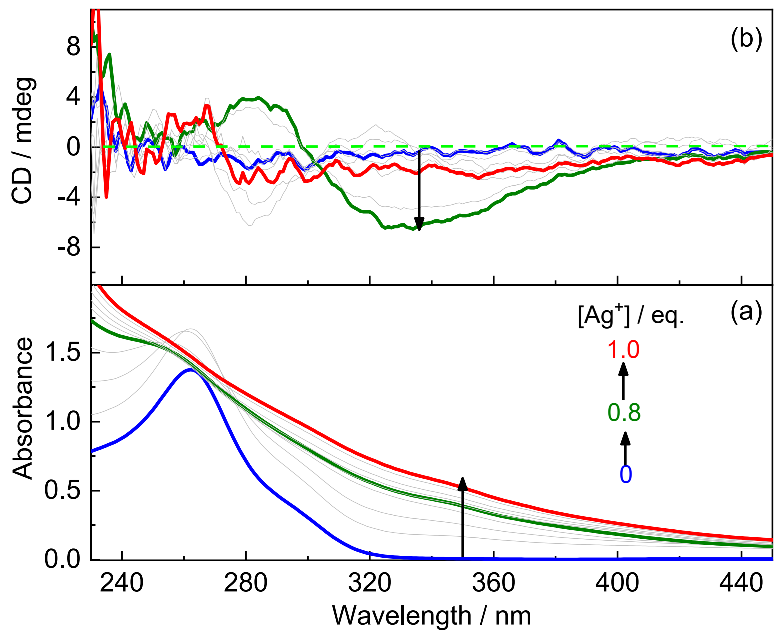

Fig. S8 Absorption (a) and CD (b) spectra of (4-MPBA+D-glucose+n-$C_8H_{17}SH$) in the presence of Ag^+ of increasing concentration in 100 mM Na_2CO_3-$NaHCO_3$ buffer of pH 10.5. [4-MPBA] = [n-$C_8H_{17}SH$] = 100 μM, [D-glucose] = 3 mM, [Ag^+] = 0 - 2.0 eq.

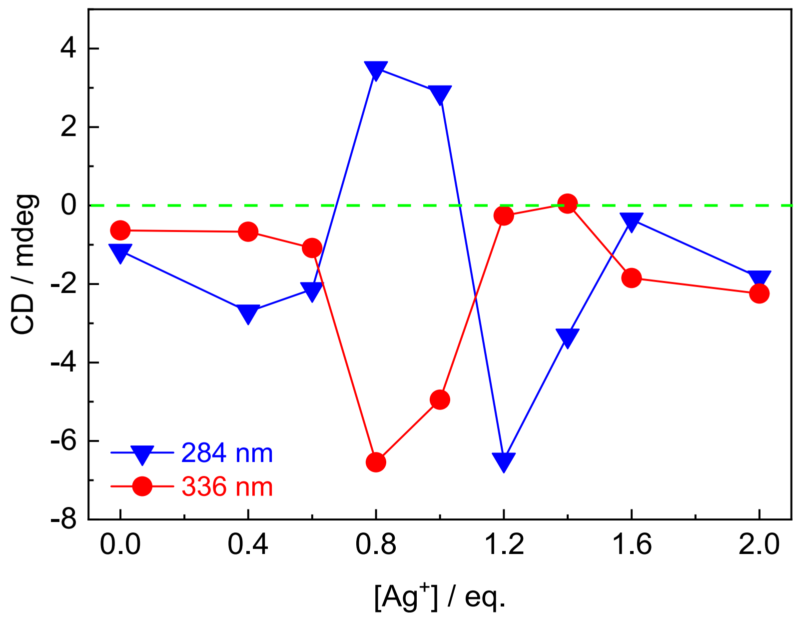

Fig. S9 Plots of CD signals of Ag^+-(4-MPBA+D-glucose+n-$C_8H_{17}SH$) in 100 mM Na_2CO_3-$NaHCO_3$ buffer solution of pH 10.5 versus equivalent of Ag^+. [4-MPBA] = [n-$C_8H_{17}SH$] = 100 μM, [D-glucose] = 3 mM, [Ag^+] = 0 - 2.0 eq.

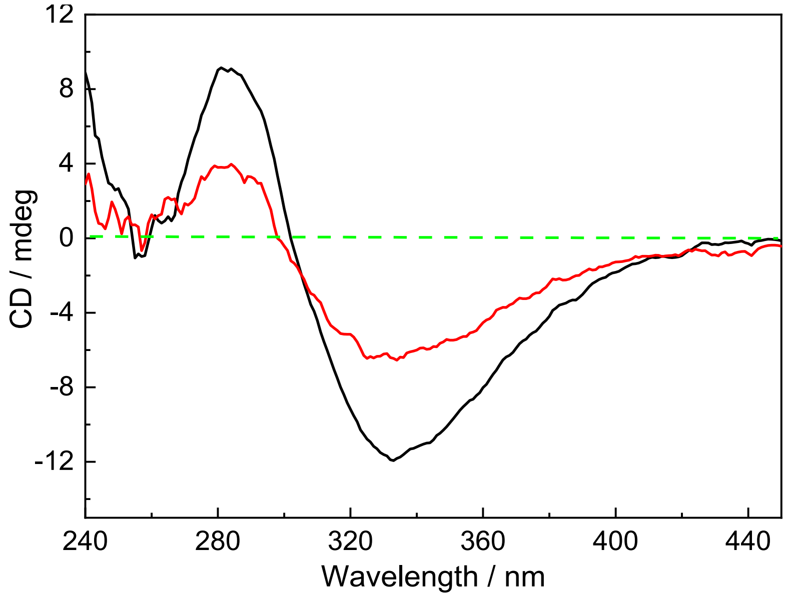

Fig. S10 CD spectra of Ag^+-(4-MPBA+D-glucose) (black line) and Ag^+-(4-MPBA+D-glucose+*n*-$C_8H_{17}SH$) (red line) in 100 mM Na_2CO_3-$NaHCO_3$ buffer solution of pH 10.5. [4-MPBA] = 100 μM, [*n*-$C_8H_{17}SH$] = 100 μM, [D-glucose] = 3 mM; [Ag^+] = 60 μM (black line), 160 μM (red line).

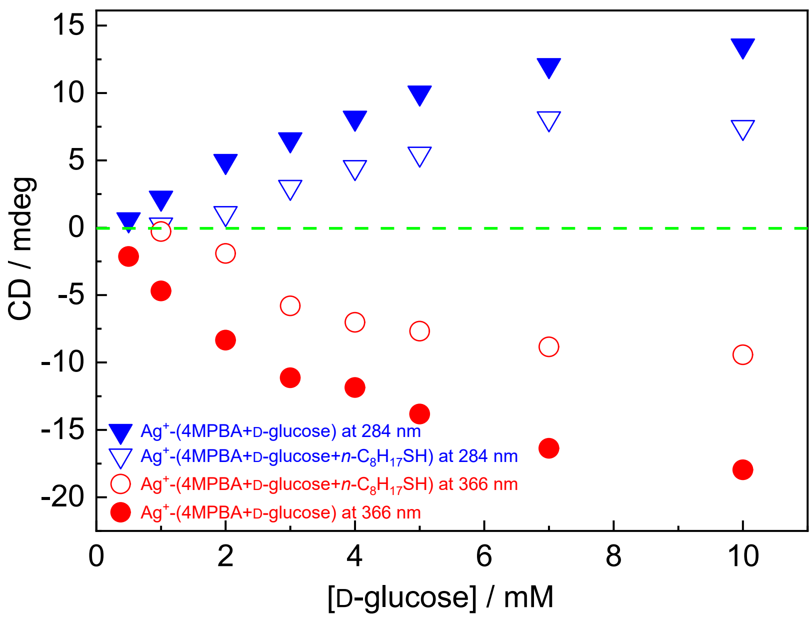

Fig. S11 Plots of CD signals of Ag^+-(4-MPBA+D-glucose) and Ag^+-(4-MPBA+D-glucose+*n*-$C_8H_{17}SH$) versus concentration of D-glucose in 100 mM Na_2CO_3-$NaHCO_3$ buffer solution of pH 10.5. [4-MPBA] = 100 μM, [*n*-$C_8H_{17}SH$] = 100 μM, [D-glucose] = 0.5 - 10 mM; [Ag^+] = 160 μM (hollow), [Ag^+] = 60 μM (solid).

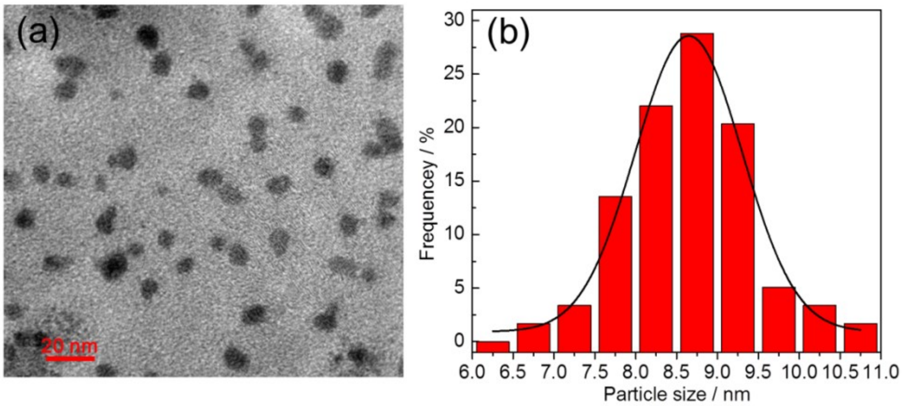

Fig. S12 TEM image (a) and size distribution (b) of Ag^+-(4-MPBA+D-glucose+*n*-$C_8H_{17}SH$) coordination polymers. [4-MPBA] = [*n*-$C_8H_{17}SH$] = 25 μM, [Ag^+] = 40 μM, [D-glucose] = 3 mM.

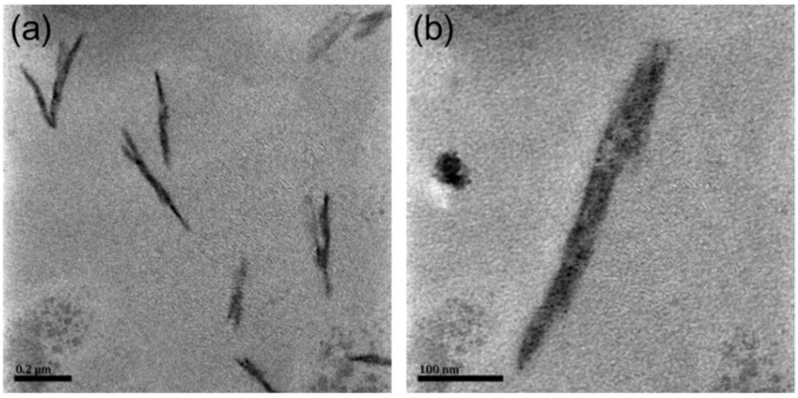

Fig. S13 TEM images of chain-like Ag^+-(4-MPBA+D-glucose) coordination polymers. [4-MPBA] = 50 μM, [Ag^+] = 30 μM, [D-glucose] = 3 mM.

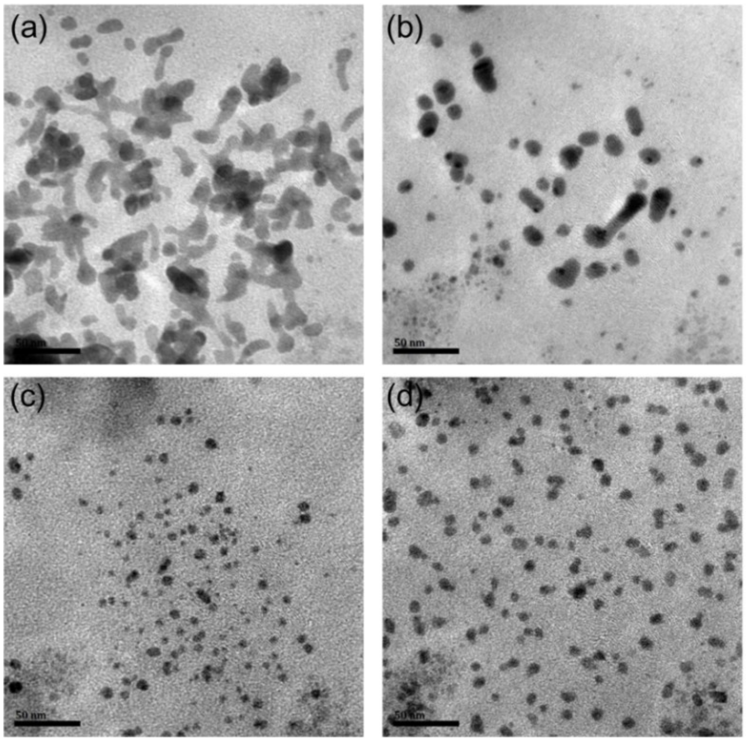

Fig. S14 TEM images of Ag^{+}-(4-MPBA+D-glucose+*n*-$C_8H_{17}SH$) coordination polymers of varying concentration of D-glucose. The samples were prepared by dropping solutions onto carbon-coated copper grids followed by solvent evaporation in vacuum. [4-MPBA] = [*n*-$C_8H_{17}SH$] = 25 μM, [Ag^{+}] = 40 μM; [D-glucose] = 0.1 mM (a), 0.25 mM (b), 0.5 mM (c), 3 mM (d).

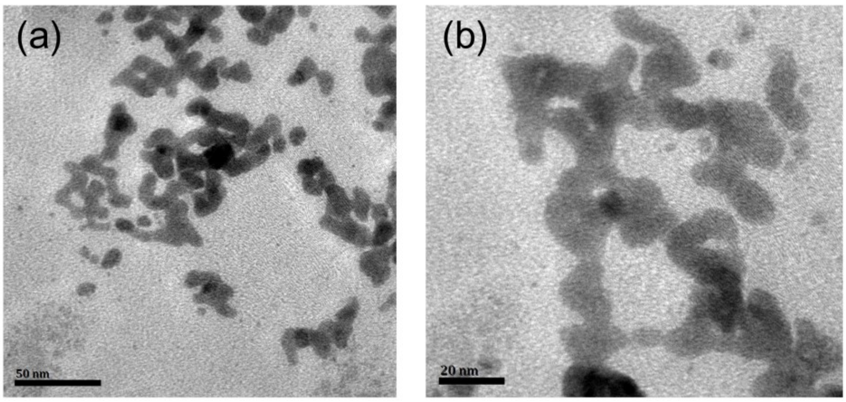

Fig. S15 TEM images of Ag^{+}-(4-MPBA+*n*-$C_8H_{17}SH$) coordination polymers. [4-MPBA] = [*n*-$C_8H_{17}SH$] = 25 μM, [Ag^{+}] = 40 μM.

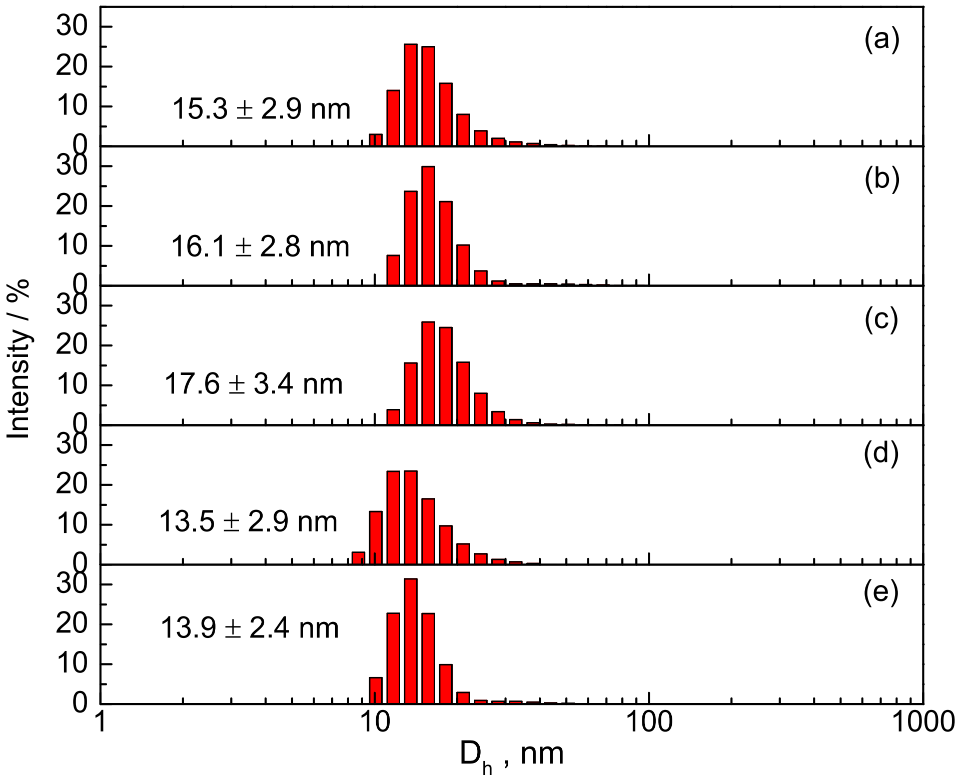

Fig. S16 DLS measured hydrodynamic diameters (D_h) of Ag^+-(4-MPBA+D-glucose+*n*-$C_8H_{17}SH$) of varying concentration in 100 mM Na_2CO_3-$NaHCO_3$ buffer of pH 10.5. [4-MPBA] = [*n*-$C_8H_{17}SH$] = 5 μM (a), 10 μM (b), 15 μM (c), 25 μM (d), 50 μM (e); [D-glucose] = 3 mM, [Ag^+] = 0.8 eq.

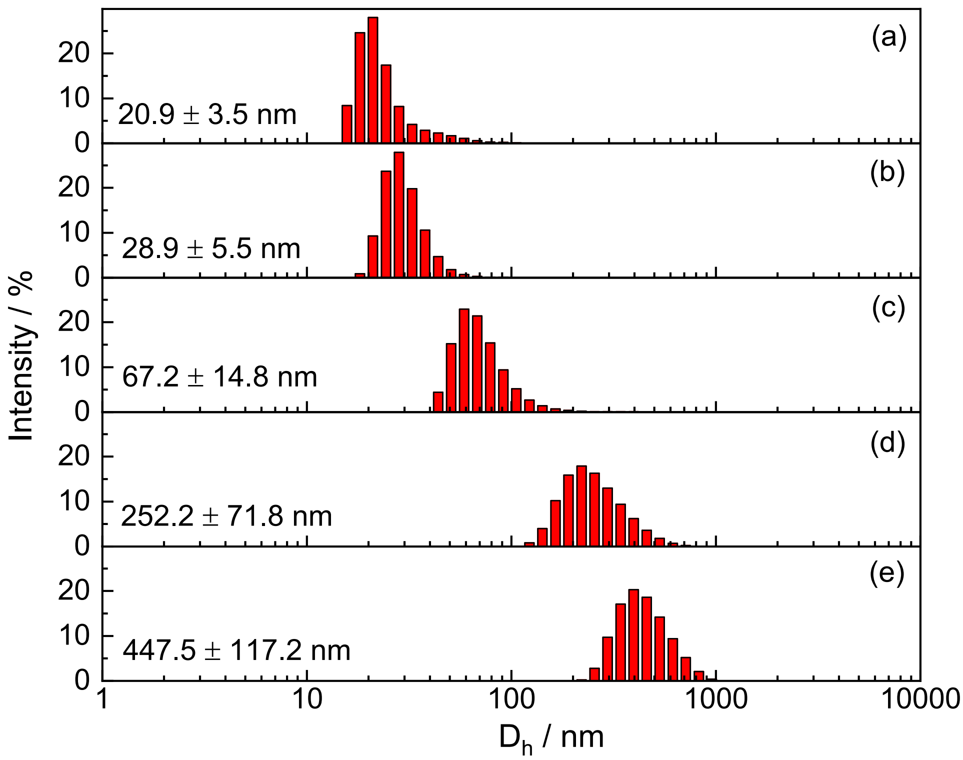

Fig. S17 DLS measured hydrodynamic diameters (D_h) of Ag^+-(4-MPBA+D-glucose) of varying concentration in 100 mM Na_2CO_3-$NaHCO_3$ buffer of pH 10.5. [4-MPBA] = 10 μM (a), 20 μM (b), 30 μM (c), 50 μM (d), 100 μM (e); [D-glucose] = 3 mM, [Ag^+] = 0.6 eq.

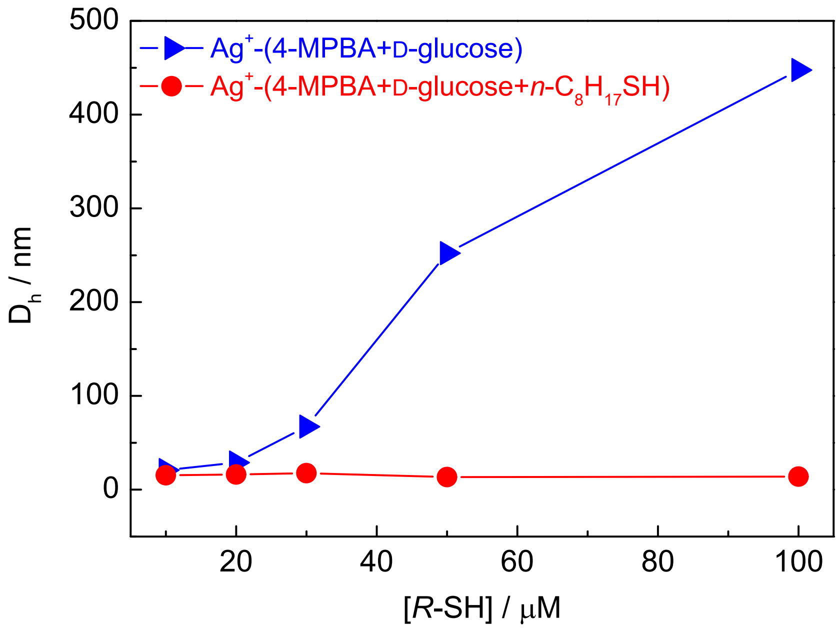

Fig. S18 Plots of DLS measured hydrodynamic diameter (D_h) of Ag^+-(4-MPBA+D-glucose) and Ag^+-(4-MPBA+D-glucose+*n*-$C_8H_{17}SH$) of varying concentration in 100 mM Na_2CO_3-$NaHCO_3$ buffer of pH 10.5. [*R*-SH] = 10 - 100 μM, [D-glucose] = 3 mM; [Ag^+] = 0.6 eq (blue), 0.8 eq (red).

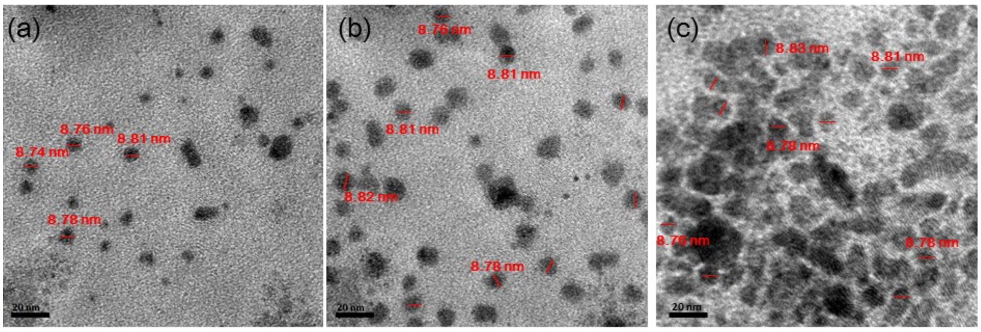

Fig. S19 TEM images of Ag^+-(4-MPBA+D-glucose+*n*-$C_8H_{17}SH$) of varying concentration in 100 mM Na_2CO_3-$NaHCO_3$ buffer solution of pH 10.5. [4-MPBA] = [*n*-$C_8H_{17}SH$] = 10 μM (a), 25 μM (b), 50 μM (c); [D-glucose] = 3 mM, [Ag^+] = 0.8 ([4-MPBA] + [*n*-$C_8H_{17}SH$]).

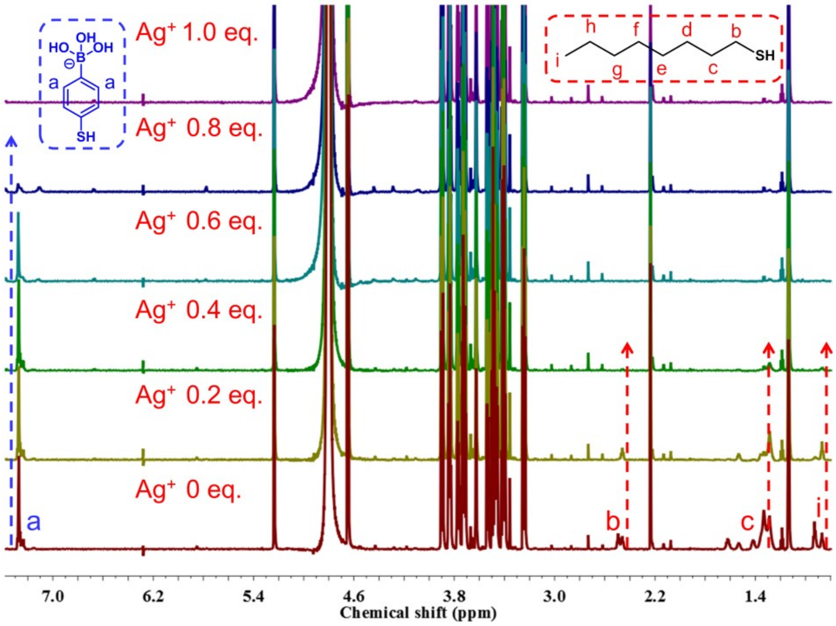

Fig. S20 Partial ^{1}H NMR spectra of Ag^+-(4-MPBA+D-glucose+*n*-$C_8H_{17}SH$) in 100 mM Na_2CO_3-$NaHCO_3$ buffer of pH 10.5 in D_2O using acetone as an internal standard. [4-MPBA] = [*n*-$C_8H_{17}SH$] = 200 μM, [D-glucose] = 3 mM; [Ag^+] = 0 - 400 μM.

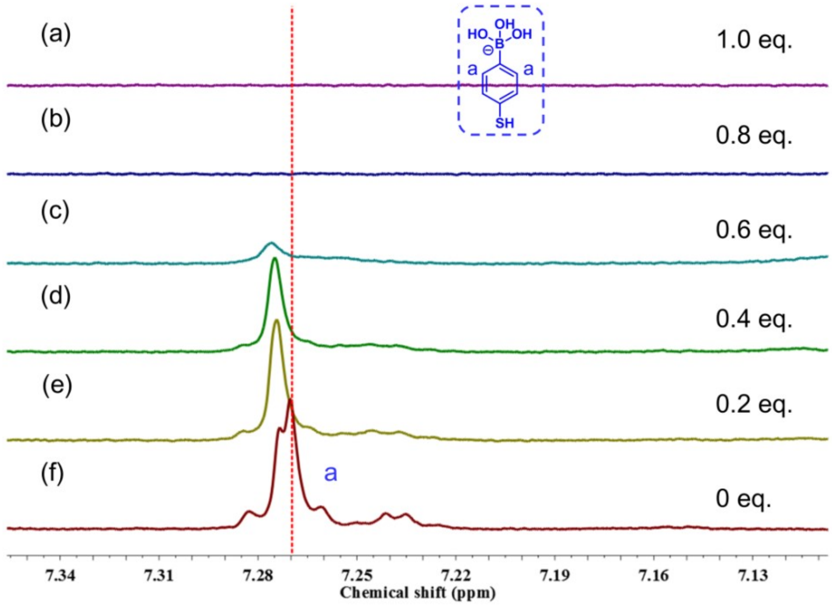

Fig. S21 Partial [1]H NMR spectra of 4-MPBA in Ag^+-(4-MPBA+D-glucose) in 100 mM Na_2CO_3-$NaHCO_3$ buffer of pH 10.5 in D_2O using acetone as an internal standard. [4-MPBA] = 200 μM, [D-glucose] = 3 mM; [Ag^+] = 0 - 200 μM.

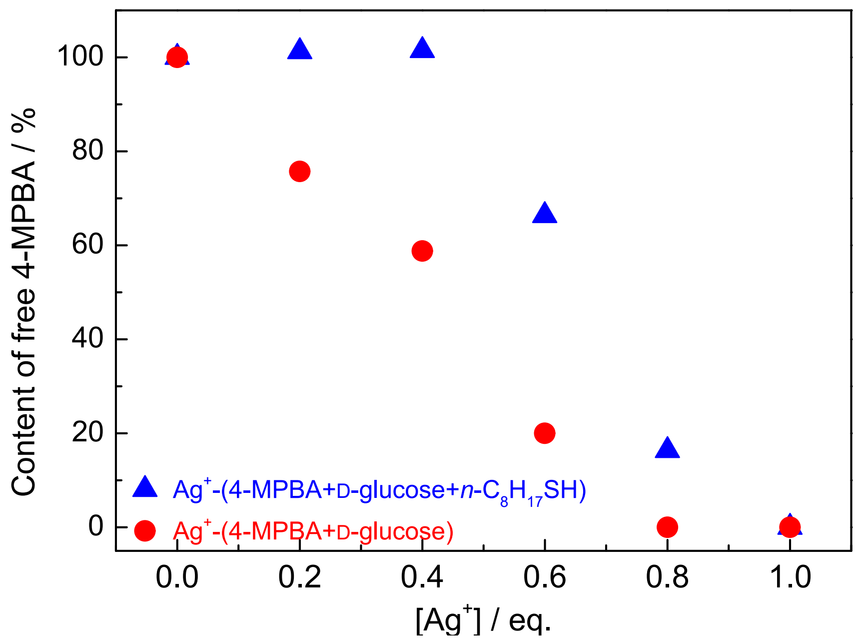

Fig. S22 Contents of free 4-MPBA calculated by [1]H NMR integrals versus added equivalent of Ag^+ of Ag^+-(4-MPBA+D-glucose+*n*-$C_8H_{17}SH$) (blue) and Ag^+-(4-MPBA+D-glucose) (red) in 100 mM Na_2CO_3-$NaHCO_3$ buffer of pH 10.5 in D_2O using acetone as an internal standard. [4-MPBA] = 200 μM, [*n*-$C_8H_{17}SH$] = 200 μM, [D-glucose] = 3 mM; [Ag^+] = 0 - 1.0 eq.

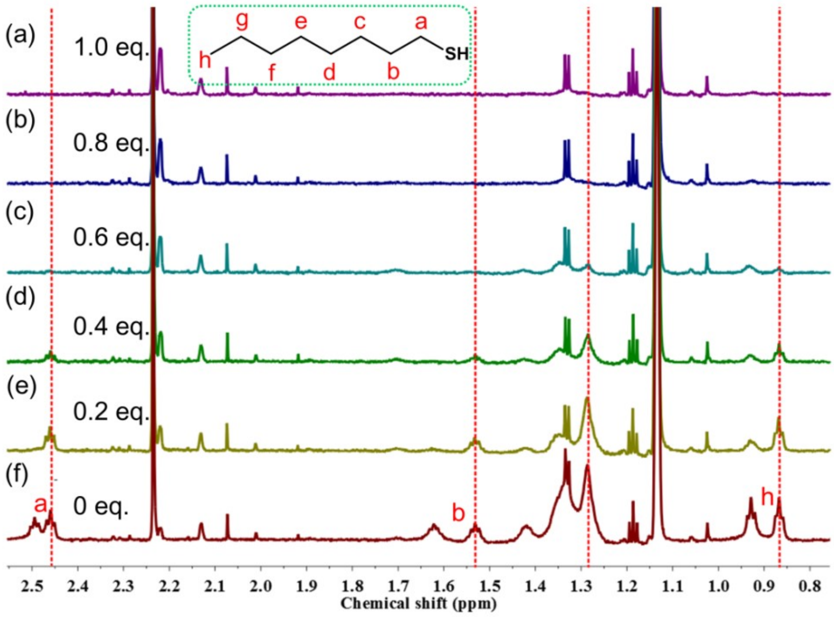

Fig. S23 Partial [1]H NMR spectra of *n*-$C_8H_{17}SH$ in Ag-SC_8H_{17}-*n* in 100 mM Na_2CO_3-$NaHCO_3$ buffer of pH 10.5 in D_2O using acetone as an internal standard. [*n*-$C_8H_{17}SH$] = 200 μM, [Ag^+] = 0 - 200 μM.

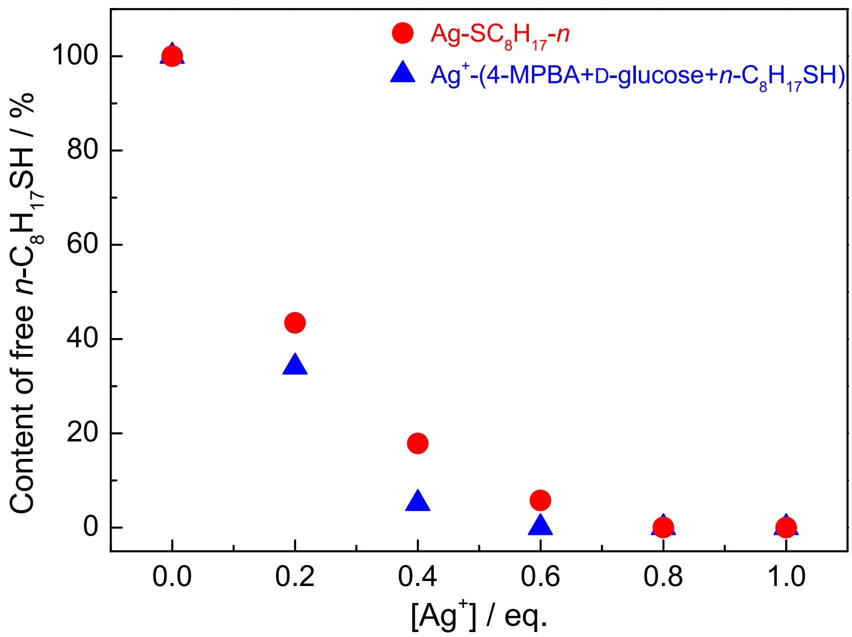

Fig. S24 Contents of free *n*-$C_8H_{17}SH$ calculated by [1]H NMR integrals versus added equivalent of Ag^+ of Ag^+-(4-MPBA+D-glucose+*n*-$C_8H_{17}SH$) (blue) and Ag-SC_8H_{17}-*n* (red) in 100 mM Na_2CO_3-$NaHCO_3$ buffer of pH 10.5 in D_2O using acetone as an internal standard. [4-MPBA] = 200 μM, [*n*-$C_8H_{17}SH$] = 200 μM, [D-glucose] = 3 mM; [Ag^+] = 0 - 1.0 eq.

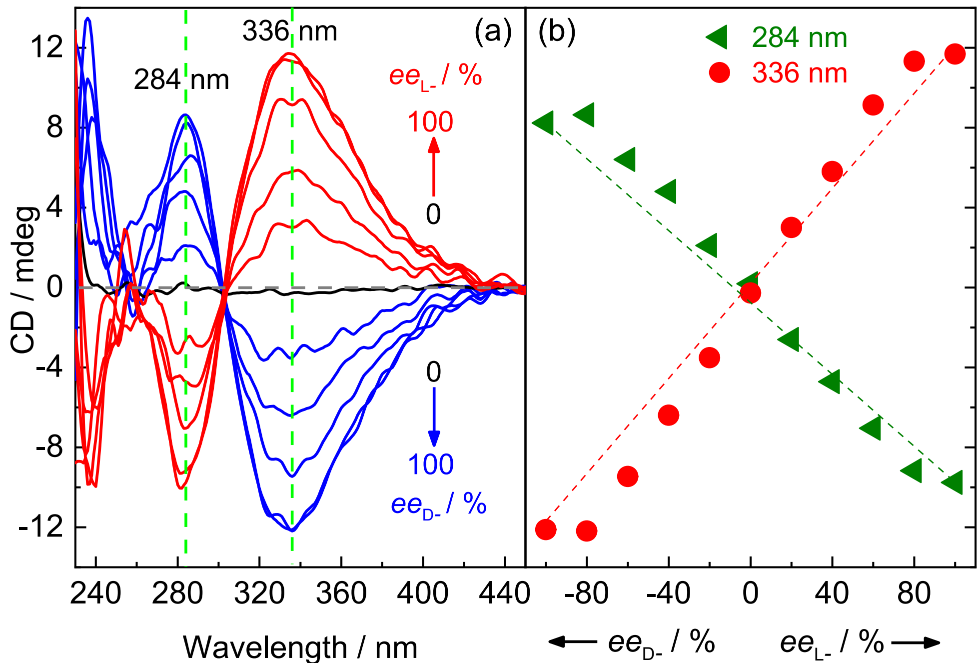

Fig. S25 (a) CD spectra and (b) plots of CD signals of Ag^+-(4-MPBA+glucose) of varying glucose *ee* in 100 mM Na_2CO_3-$NaHCO_3$ buffer of pH 10.5. [4-MPBA] = 100 μM, [Ag^+] = 60 μM, [D-glucose] + [L-glucose] = 4 mM.

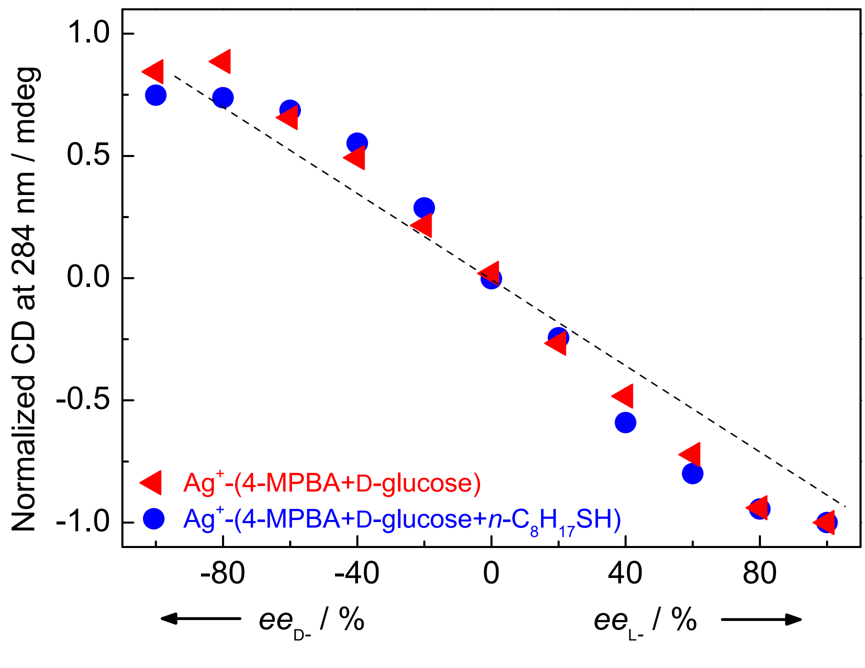

Fig. S26 Plots of normalized CD signals at 284 nm of Ag^+-(4-MPBA+D-glucose) and Ag^+-(4-MPBA+D-glucose+n-C_8H_{17}SH) versus *ee* of glucose in 100 mM Na_2CO_3-$NaHCO_3$ buffer of pH 10.5. [4-MPBA] = [n-C_8H_{17}SH] = 100 μM, [D-glucose] + [L-glucose] = 4 mM; [Ag^+] = 160 μM (blue), 60 μM (red).

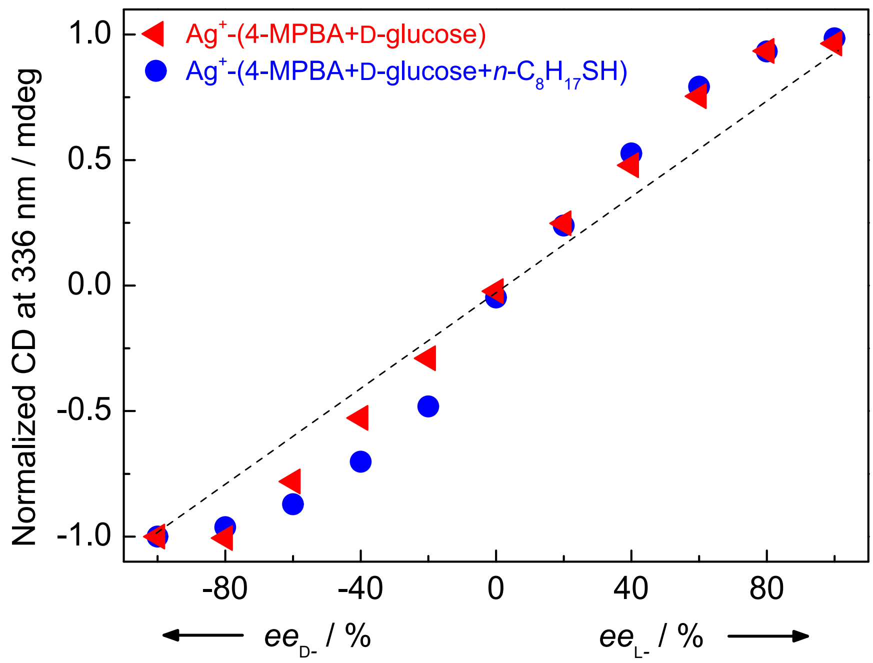

Fig. S27 Plots of normalized CD signals at 336 nm of Ag^+-(4-MPBA+D-glucose) and Ag^+-(4-MPBA+D-glucose+n-$C_8H_{17}SH$) versus *ee* of glucose in 100 mM Na_2CO_3-$NaHCO_3$ buffer of pH 10.5. [4-MPBA] = [n-$C_8H_{17}SH$] = 100 μM, [D-glucose] + [L-glucose] = 4 mM; [Ag^+] = 160 μM (blue), 60 μM (red).

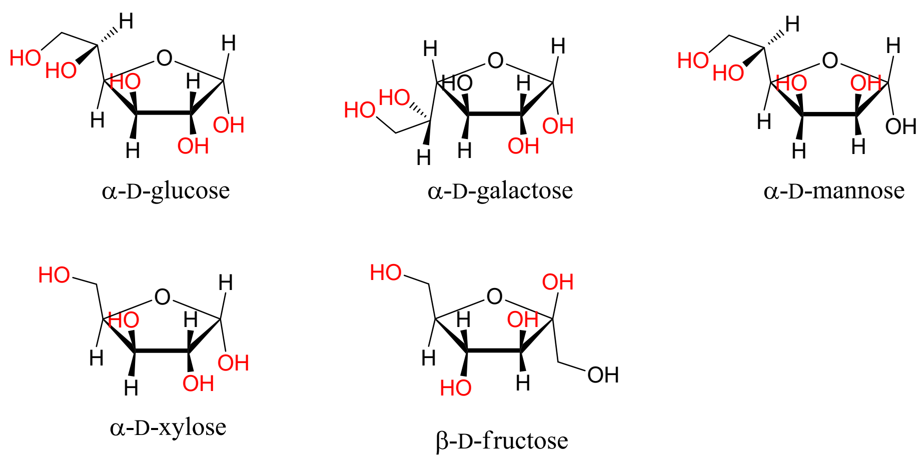

Scheme S2 Chemical structures of the tested monosaccharides

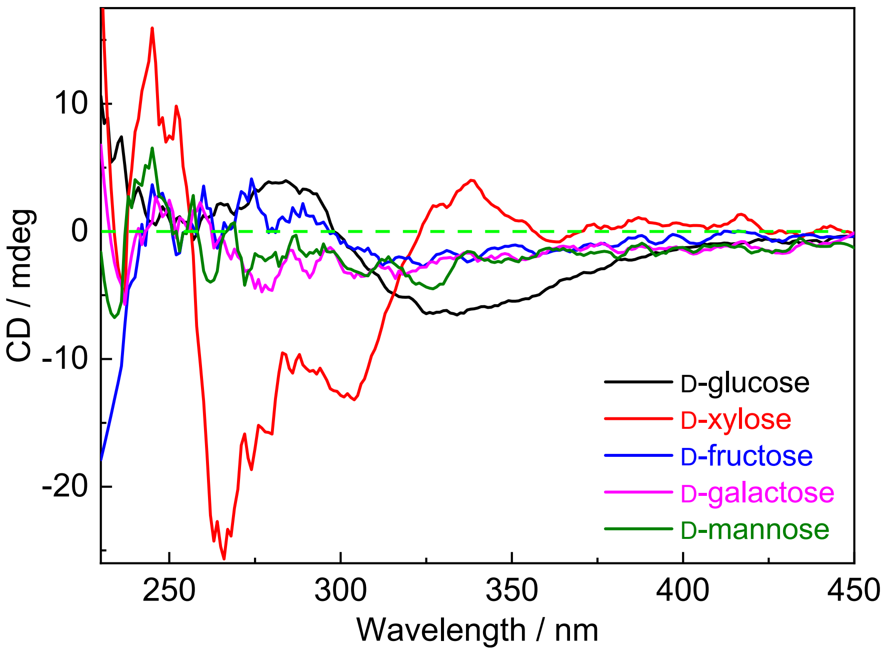

Fig. S28 CD spectra of Ag^+-(4-MPBA+D-monosaccharide+*n*-$C_8H_{17}SH$) in 100 mM Na_2CO_3-$NaHCO_3$ buffer of pH 10.5. [4-MPBA] = [*n*-$C_8H_{17}SH$] = 100 μM, [D-monosaccharide] = 3 mM, [Ag^+] = 160 μM.

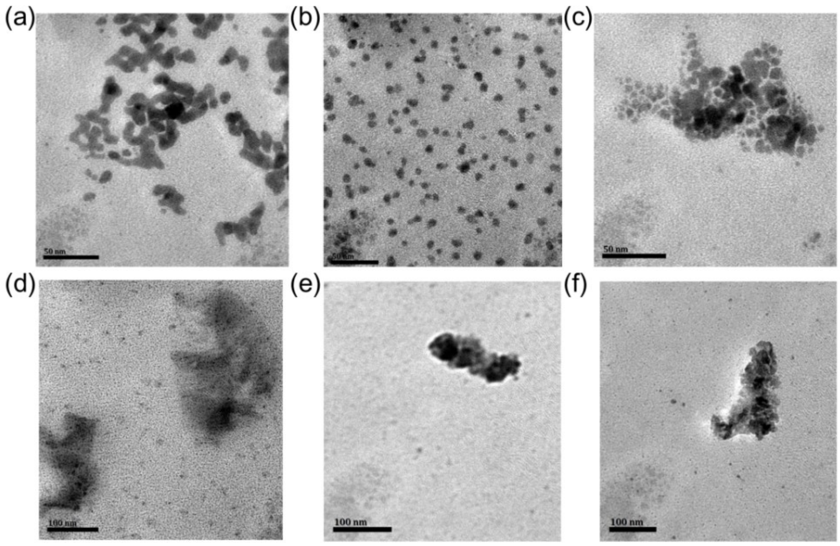

Fig. S29 TEM images of (a) Ag^+-(4-MPBA+*n*-$C_8H_{17}SH$) and (b-f) Ag^+-(4-MPBA+D-monosaccharide+*n*-$C_8H_{17}SH$). Monosaccharide = D-glucose (b), D-xylose (c), D-fructose (d), D-galactose (e) or D-mannose (f). [4-MPBA] = [*n*-$C_8H_{17}SH$] = 25 μM, [Ag^+] = 40 μM, [D-monosaccharide] = 3 mM.

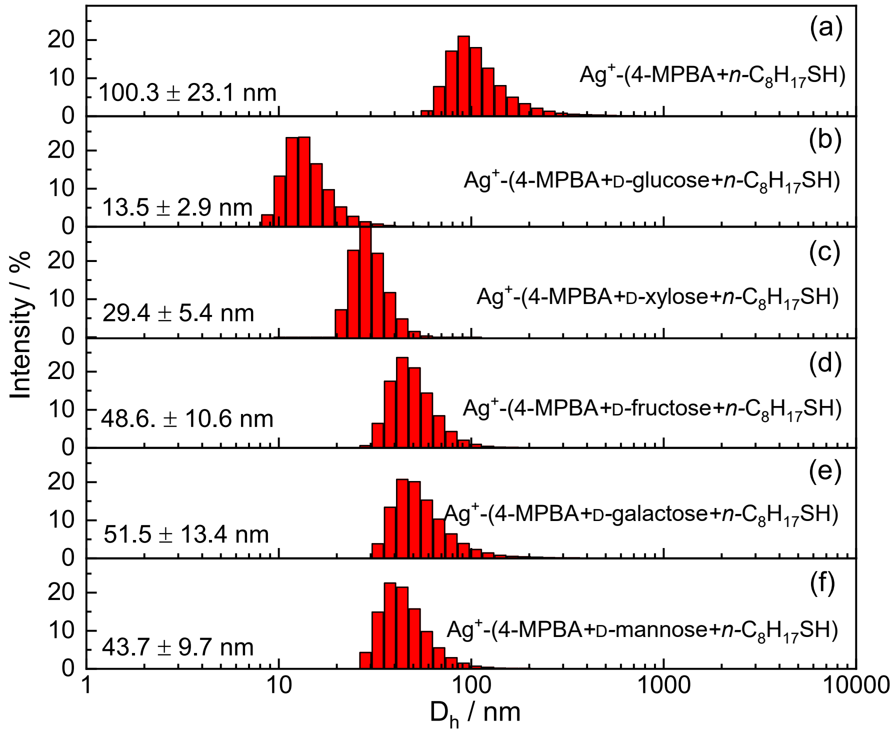

Fig. S30 DLS measured hydrodynamic diameters (D_h) of Ag^+-(4-MPBA+*n*-C_8H_{17}SH) polymers (a) and Ag^+-(4-MPBA+D-monosaccharide+*n*-C_8H_{17}SH) of monosaccharide being (b) D-glucose, (c) D-xylose, (d) D-fructose, (e) D-galactose or (f) D-mannose. [4-MPBA] = [*n*-C_8H_{17}SH] = 25 μM, [Ag^+] = 40 μM, [D-monosaccharide] = 3 mM.